RADIO SCIENCE Journal of Research NBS/USNC–URSI
Vol. 68D, No. 2, February 1964

Diurnal Phase Variation of VLF Waves at Medium Distances

Hans Volland

Contribution from Heinrich-Hertz-Institut, Berlin-Charlottenburg, Germany

(Received August 12, 1963)

Methods of phase measurements at VLF are briefly described. Some results of diurnal phase measurements, sunrise effects, and solar flare effects at medium distances and northern geographical latitudes are summarized. Two inhomogeneous and anisotropic models are used for the interpretation of the measurements: the first corresponding to the daytime ionosphere and the second corresponding to the nighttime ionosphere. The models are related to homogeneous models with sharp boundaries and effective parameters of conductivity, dielectric constant, and equivalent height. The diurnal phase lag, depending on distance, and the sunrise effects at 1000 km and 2000 km are interpreted by these models. Two critical distances exist where the nighttime phase gains a phase advantage of 360 degrees relative to the daytime phase. An electron profile of the daytime lower ionosphere is deduced from measured daytime variations of equivalent height. The strength of ionizing solar radiation during a solar flare and the effective attachment coefficient of the lower ionosphere are derived from measured variations of the equivalent height during a solar flare.

1. Introduction

VLF waves (3 to 30 kc/s) are increasingly used as communication medium for time and frequency comparison and for long range navigation systems. In all these cases, the frequency of a cw-transmitter is compared with the frequency of an oscillator at the recieving station, which is independent of the transmitter oscillator.

VLF wave propagation takes place in the waveguide between earth's surface and the lower ionosphere. This waveguide behaves as a transformer and depends on frequency, time, and location. Each change of the transformer characteristics of the wave guide is accompanied by a change of phase of the transmitter at the receiving station relative to the receiver oscillator. Therefore, the transformer characteristics and their variations must be known in any practical application.

In the atmospheric waveguide primary, the reflection characteristics and the equivalent height of the lower ionosphere vary. On the other hand, the influence of the inhomogeneous earth's surface, with different coverings in winter and summer, is of subordinate importance. Therefore, VLF waves are a very useful tool for studying the lower ionosphere.

Observations of VLF propagation at medium distances are especially suitable for this research because the strong influence of the skywaves increases as to distance increases while the earth's magnetic field has only a small effect. Otherwise, the region of propagation behaves nearly as a space which is homogeneous in the horizontal direction. Therefore, it is possible to use a relatively simple model for the theoretical interpretation.

Medium distances shall be distances where the propagation of electromagnetic energy does not take place predominantly by one mode. At daytime this range comprises of distances between about 300 and 3000 km. Within 300 km the principal wave is the groundwave. Beyond 3000 km the first waveguide mode is the chief carrier of energy. At nighttime the range becomes larger because of the smaller absorption of the ionospheric skywaves.

A great deal of early work of VLF research has been done by the Cambridge group. The results are summarized by Bracewell et al., [1951]. The easiest method of phase measurement is to lock the receiver oscillator with the transmitter oscillator, e.g., by telephone circuits [Bracewell, 1952]. Naturally this is possibly only for relatively short distances and suitable local conditions. Pierce [1955, 1957] compared the frequency of an independent oscillator in Cambridge (Mass.) with the highly stabilized frequency of GBR (Rugby), 16 kc/s, and first realized useful phase measurements over large distances.

This paper reports results of diurnal phase measurements at medium distances and their interpretation. Attention is restricted to regular changes including sunrise effects and solar flare effects, but does not discuss nighttime anomalies like magnetic storm effects or cosmic ray effects. The reason, therefore, is that the nighttime ionosphere is very unstable and becomes highly inhomogeneous in the horizontal direction at such anomalies, consequently a quantitative interpretation is extremely difficult. Since only the phase together with the amplitude of the field strength gives unique information, it is sometimes inevitable for the interpretation of the measurements to use the amplitude too.

2. Results of Phase Measurements

2.1. Method of Phase Measurement

The phase of a transmitter at the receiving station has the form

$$\Omega=\omega t-k\rho+\varphi(\rho,t) \tag{1}$$

where $\varphi(\rho,t)$ is a variable form which depends on both range, ρ, and time, t. The receiver oscillator has the phase

$$\Omega_E=\omega_E t+\varphi_E. \tag{2}$$

Here ω and ω_E are the angular frequencies of the transmitter and the receiver oscillator, respectively; t is the time; $k=\omega/c$ is the wave number; c is the velocity of light; and ρ is the distance between transmitter and receiver. The phase

$$\omega t-k\rho=\omega(t-\rho/c) \tag{3}$$

is the phase of an undisturbed wave propagating in free space; $\varphi(\rho, t)$ is the phase difference from this ideal value; and φ_E is an arbitrary phase constant of the receiver oscillator.

If the two frequencies are mixed in a converter, a difference frequency will be obtained, and the resulting phase difference is

$$\Omega-\Omega_E=(\omega-\omega_E)t+\varphi(\rho, t)-k\rho-\varphi_E. \tag{4}$$

Since the oscillators of the transmitter and the receiver generally are not synchronized, the result of phase measurement is undecided by the factor

$$k\rho+\varphi_E. \tag{5}$$

Furthermore, each frequency difference of the two oscillators gives a linear phase change with time which adds to the diurnal variation $\varphi(\rho, t)$. Often the frequency of the receiver oscillator changes by

$$\omega_E=\omega_{E0}+\alpha t. \tag{6}$$

Then the phase change with time even is of parabola form. Such an oscillator run can be compensated [Utech and Zahn, 1961].

The maximal diurnal change of φ is of the order

$$|\varphi_{\text{day}}-\varphi_{\text{night}}|=2\pi. \tag{7}$$

In order to measure primary, the change of φ it must yield within one daily interval ($T\approx 10^5$ sec)

$$(\omega-\omega_E)T<<2\pi$$

or

$$\frac{\Delta f}{f}<<\frac{1}{fT}. \tag{8}$$

At the frequency $f=10$ kc/s we get

$$\frac{\Delta f}{f}<<10^{-9}. \tag{9}$$

The frequencies of the oscillator must be stabilized at least for 1 in 10^{10}, if a useful diurnal phase measurement at VLF shall be possible. The method of achieving this extreme condition is beyond the scope of this paper. Details may be found in Pierce [1957], Crombie et al. [1958], and Eppen and Heydt [1959].

An accuracy of 1 in 10^{10} of the oscillator frequency is already the upper limit which can be realized within economic limitations. The oscillator of GBR (16 kc/s) has this accuracy [Pierce et al., 1960]. Therefore, the determination of the reference phase is not unique. Yet, the experiments show that the lower ionosphere at daytime is rather stable, and its behavior at midday only is changing a little from day to day. This is the reason that the phase value at midday will be used as reference phase.

The following data will show the phase difference

$$\Delta\varphi=\varphi-\varphi_{\text{midday}}, \tag{10}$$

although for some purposes the time delay,

$$\Delta\tau=\frac{\Delta\varphi}{\omega}, \tag{11}$$

is used when measurements at different frequencies are compared. Finally, the phase lag is defined by

$$-\Delta\varphi=\varphi_{\text{midday}}-\varphi. \tag{12}$$

2.2. Results of Diurnal Phase Measurements

Figure 1 shows results of phase measurements of GBR (16 kc/s) in Berlin for the year 1962. The distance between transmitter and receiver is 980 km. The monthly means of hourly median values of $\Delta\varphi$ are scaled versus time of day. The propagation path is directed nearly from west to east. The shift of the daytime maximum and the shift of the nighttime minimum to earlier hours than midday and midnight, respectively, are striking. The difference time of sunrise or sunset at the locations of the transmitter and receiver is smaller than 1 hr. The variation of phase must be caused, therefore, by a smooth variation of the equivalent reflection height and the reflection characteristics of the lower ionosphere. On the other hand, Pierce [1957] and Chilton et al. [1962], find a trapezium shape of the diurnal phase variation for greater distances. The duration of the slope of the trapezium depends on the time during which parts of the propagation path lie in twilight. The duration becomes great for propagation paths directed from east to west or vice versa and are small for paths directed from south to north or vice versa.

If only the first mode is the carrier of energy (for distances greater than about 3000 km), it is sufficient for an approximate interpretation of the transition to assume that the phase of the mode is propagating with a constant phase velocity at daytime and a

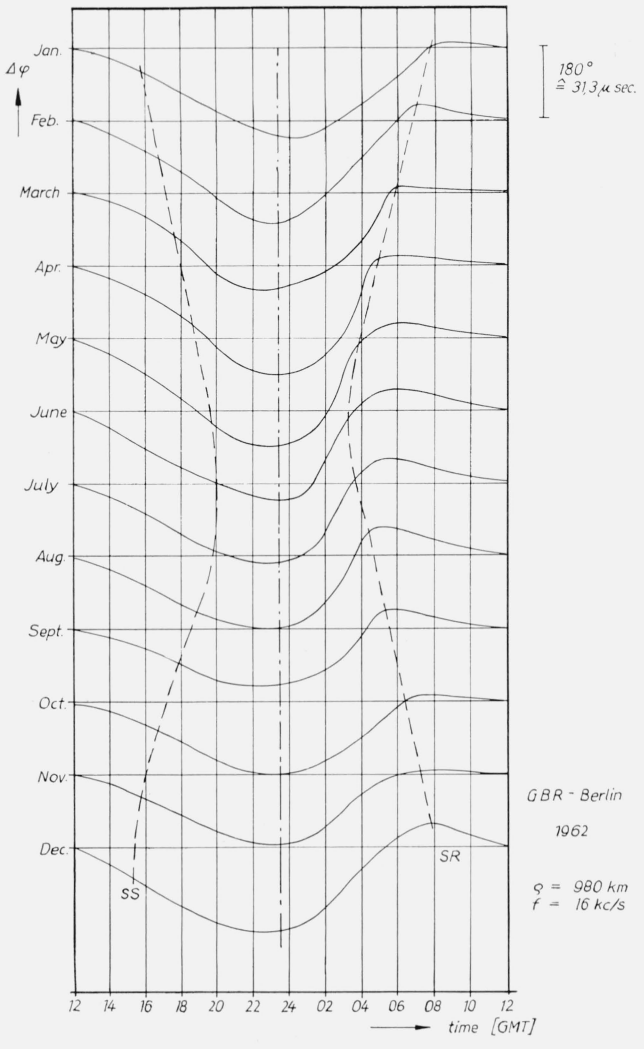

FIGURE 1. *Monthly means of diurnal phase difference* $\Delta\varphi$ *of GBR versus time observed in Berlin during the year 1962.*

The dashed lines indicate time of sunrise (SR) and time of sunset (SS), the dash-dotted line indicates time of midnight at the middle of the propagation path.

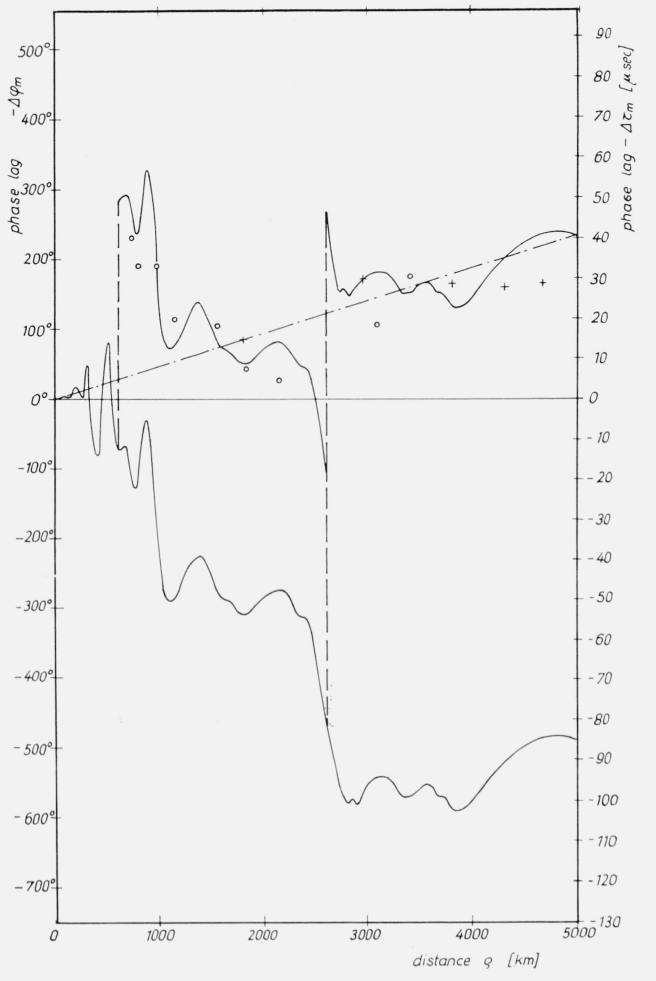

FIGURE 2. *Calculated maximal diurnal phase lag* $-\Delta\varphi_m$ *versus distance of a 16 kc/s transmitter (full lines).*

For details see text. The circles are measured 16 kc/s values, the crosses are measured 18 kc/s values.

different constant phase velocity at nighttime. In regions of transition from night to day, the portions of phase paths are simply added. For example, if p is the percentage portion of the nighttime phase path, then the whole phase at the receiver is [Crombie et al., 1958]

$$\Omega=\omega t-(1-p)(k\rho-\varphi_{\mathrm{day}})-p(k\rho-\varphi_{\mathrm{night}}), \quad (13)$$

and thus

$$\Delta\varphi=p\Delta\varphi_m, \quad (14)$$

where

$$\Delta\varphi_m=\varphi_{\mathrm{night}}-\varphi_{\mathrm{day}} \quad (15)$$

is the measured maximal phase difference relative to the phase at midday. Since the change of p is approximately linear, (14) gives a trapezium variation.

With help of (14), Blackband [1962] and Hampton and Hill [1962] were able to explain the daily phase variations over propagation paths crossing arctic regions. In winter or summer there exist two extremes of daily phase variation, because parts of the propagation paths are dark and illuminated, respectively, during the whole day. For shorter distances, the propagation must be interpreted by ray theory. Here it is better to describe the transition from night to day by a steady change of the ionospheric characteristics over the whole propagation path (see sec. 3.4).

Casselman et al., [1959], Blackband [1962b], and Westfall [1961] have reported the maximum phase lag $-\Delta\varphi_m$ for different distances from the transmitter and different frequencies between 10 and 20 kc/s. Some of these results for the frequencies 16 and 18 kc/s together with the data from figure 1 and 3 are plotted versus distance ρ in figure 2.

Contrary to the presentation of these data by Blackband, no attempt has been made to eliminate

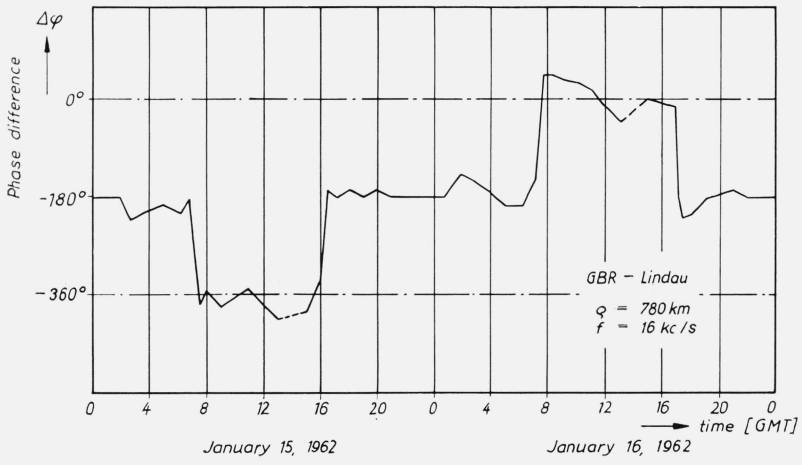

FIGURE 3. *Diurnal phase difference $\Delta\varphi$ of GBR versus time measured in Lindau (Germany).*

the groundwave at smaller distances. For 18 kc/s, only the right scale $-\Delta\tau_m$ is significant. In all cases the vertical component of the field strength E_z has been measured. The strong minimum of phase lag in the region between 2000 and 2500 km is striking.

For all distances, the measured values $\Delta\tau_m$ are negative. A remarkable exception from this rule has been observed in Lindau (Germany). Figure 3 shows two successive daily phase variations of GBR. On the first day there exists the normal behavior of variation (plotted in fig. 2) which fits to the other values. The next day an inversion of phase lag is observed. The maximum difference of phase on both days is about 360°. Such phase inversions are rare and have been observed up to now only at distances round 700 km from the transmitter.

Blackband [1962b] has shown that for great distances the value $-\Delta\tau_m/\rho$ is nearly constant at constant frequency and decreases with frequency down to a minimum at about 16 kc/s. In figure 4 the measured values are plotted versus frequency.

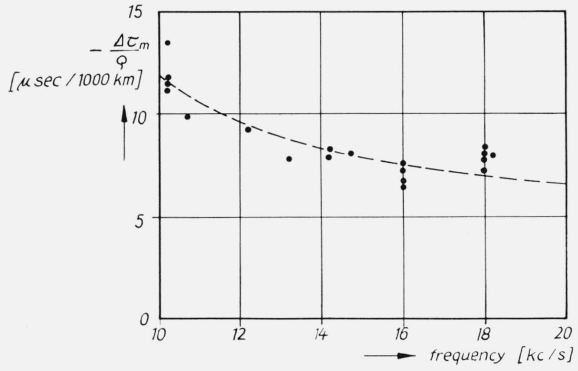

FIGURE 4. *Calculated values $-\Delta\tau_m/\rho$ versus frequency (dashed line).*

The points are measured values according to Blackband [1962b].

Blackband did not find any significant dependence of this data on direction of propagation (influence of earth's magnetic field) or propagation path (influence of the distribution of continents and oceans).

2.3. Sunrise Effects

At medium distances the sunrise effects are very regular and marked in phase and amplitude of VLF. The sunset effects are much weaker and not so regular. As a result of the averaging in figure 1, the sunrise effects are smoothed out. Two examples of sunrise effects of GBR, measured in Berlin, are shown in figure 5. The ordinates are the monthly means of July and December 1962, respectively, with phase and amplitude separated. The abscissa is the time difference centered to the time of zenith distance $\chi=96°$ at the middle of the propagation path. That is equivalent with the time of sunrise in 35 km height above the middle of the path. In summer a deep minimum of amplitude and a turning point of phase can be seen; in winter there is a maximum followed by a minimum in amplitude and likewise a turning point in phase. The beginning of the sunrise effect is at about $\chi=99°$. This corresponds to sunrise at the height of 80 km above the middle of the path. At 2000 km the phase of sunrise effect can surpass the daily variation as Blackband [1961] has shown (see fig. 13).

2.4. Solar Flare Effects

A solar flare lowers the whole daytime portion of the lower ionosphere. The homogeneous conditions, therefore, will not change during a solar flare, and the same theoretical model which is valid for the normal daily variations can be accepted for its interpretation. The decrease of equivalent height and the change of the reflection coefficient of the lower ionosphere during a solar flare changes the

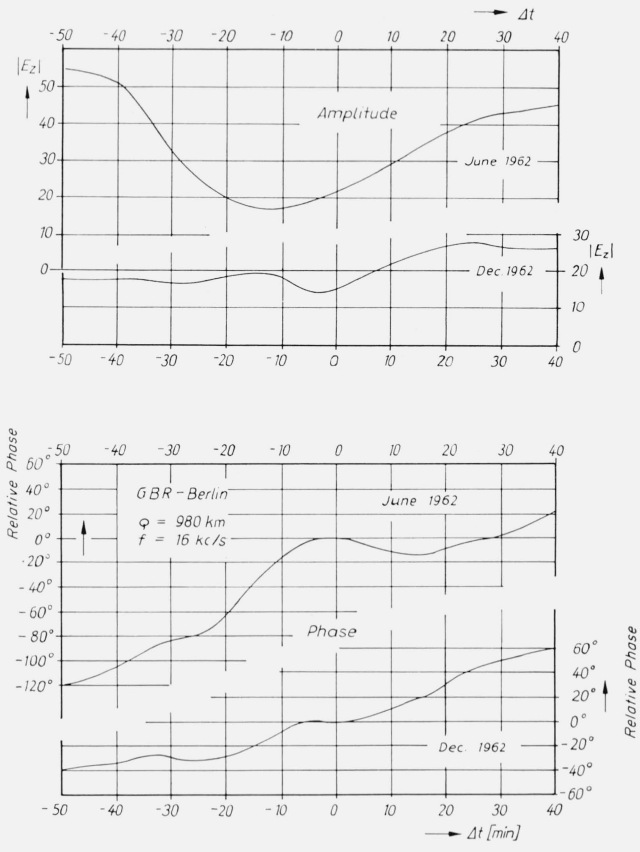

FIGURE 5. *Monthly means of phase and amplitude of electric field strength of GBR during sunrise measured in Berlin in June 1962 and December 1962.*

The time difference Δt is centered to the time of sunrise in 35 km height above the middle of the propagation path.

interference pattern between groundwave and skywaves. The change of phase, the well-known sudden phase anomaly (SPA), generally is positive. The change of amplitude can become positive or negative depending on frequency, distance, and time of day [Volland, 1959].

Figure 6 gives an instructive example of three successive solar flares on GBR measured in Berlin. All three effects are recognized uniquely as solar flare effects by other independent, simultaneous, solar-terrestrial events and show an increase of phase indicating a decrease of equivalent height. The amplitude changes otherwise are positive, negative, and zero, because the mutual phase of the groundwave and the one hop wave becomes slightly negative, positive, or zero.

3. Interpretation of Phase Measurements

3.1. Ionospheric Model

The results of phase measurements mentioned above can be explained in their essential features with the help of VLF propagation theories. These theories presume that the region between earth's

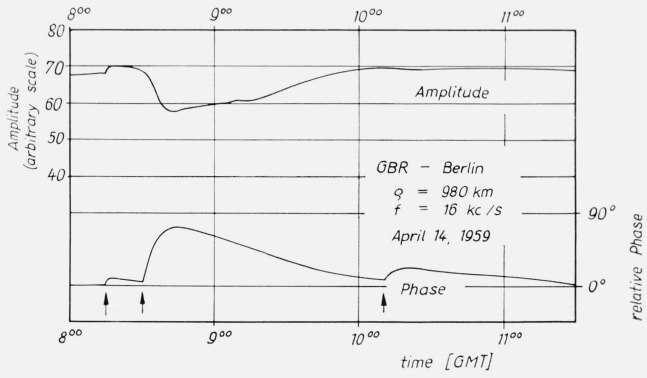

FIGURE 6. *Amplitude and phase of GBR field strength observed in Berlin during three successive solar flares.*

The arrows indicate the beginning of the effects.

surface and ionosphere is a plane or curved waveguide with sharp bounded homogeneous walls. Electromagnetic energy in such a waveguide can propagate only in discrete modes. Solely for short distances, the familiar ray theory of wave propagation is a suitable approximation. The transition between ray theory and mode theory occurs at medium distances for VLF waves. Both theories give the same results in the transition region [Volland, 1961].

The diurnal phase lag depending on distance can be explained for greater distances according to Wait [1961], Westfall [1961], and Crombie et al., [1958] as the difference between daytime phase velocity and nighttime phase velocity of the first mode. This is caused by the change of equivalent height of reflection from about 70 km at daytime to about 90 km at nighttime. Thereby the curvature of the earth's surface is important, since within a curved waveguide, the effective distance between transmitter and receiver changes with the height of the waveguide. In this connection, Wait [1963] explained, qualitatively, the phase lag minimum in figure 2 as the interference between first and second mode. On the other, the frequency dependence of $\Delta\tau_m/\rho$ in figure 4 may be interpreted in terms of frequency dependence of the propagation constant of the first mode [Blackband, 1962b]. In fact, Wait [1963] explains the measured minimum in figure 4 by the exact mode theory of curved waveguides.

In this section the ionosphere is considered as plane, but anisotropic and inhomogeneous in vertical direction. Concepts like equivalent height, effective conductivity, and effective dielectric constant will be connected with realistic ionospheric models. Since most of the phase measurements have been made with the transmitter GBR (Rugby), the calculations will be restricted to ionospheric models in medium northern geographical latitudes and to the frequency 16 kc/s. We expect results which are at least typical for VLF waves outside the equatorial regions. Detailed calculations of VLF

propagation valid for the equatorial zones have been made by Crombie [1960, 1961].

We assume a Chapman profile,

$$N=N_m \exp\{(1/2)(1-\exp[(z_m-z)/H])\}, \quad (16)$$

taking into consideration a recombination coefficient decreasing exponentially with height and a collision number profile according to Nicolet [1959] which behaves approximately as

$$\nu=\nu_0 \exp[(z_0-z)/H]; \qquad \begin{aligned} \nu_0&=10^7 s^{-1} \\ z_0&=70 \text{ km} \\ H&=8 \text{ km} \end{aligned} \quad (17)$$

below 90 km. We neglect the difference between ν and the effective value of ν at low frequencies which may differ by a factor 2 [Ginzburg, 1961], because already the data of Nicolet are rather uncertain, and ν itself surely varies with location and season. The earth's magnetic field is assumed to be vertical with the value of the (angular) gyromagnetic frequency at medium northern latitudes

$$\omega_H=8\cdot 10^6 s^{-1}.$$

For this model, and a set of parameters N_m and z_m, the elements of the reflection matrix

$$\mathbf{R}=\begin{pmatrix} {}_{\parallel}R_{\parallel} & {}_{\parallel}R_{\perp} \\ {}_{\perp}R_{\parallel} & {}_{\perp}R_{\perp} \end{pmatrix} \quad (18)$$

of plane electromagnetic waves depending on angle of incidence have been calculated [Volland, 1963]. Since the penetration depth of VLF waves at daytime is of the order of one wavelength, the ionosphere above the D layer has only a small influence on the reflection characteristics and can be neglected. At nighttime the VLF waves can penetrate into the higher ionosphere. The calculated reflection coefficients of the nighttime ionosphere, therefore,

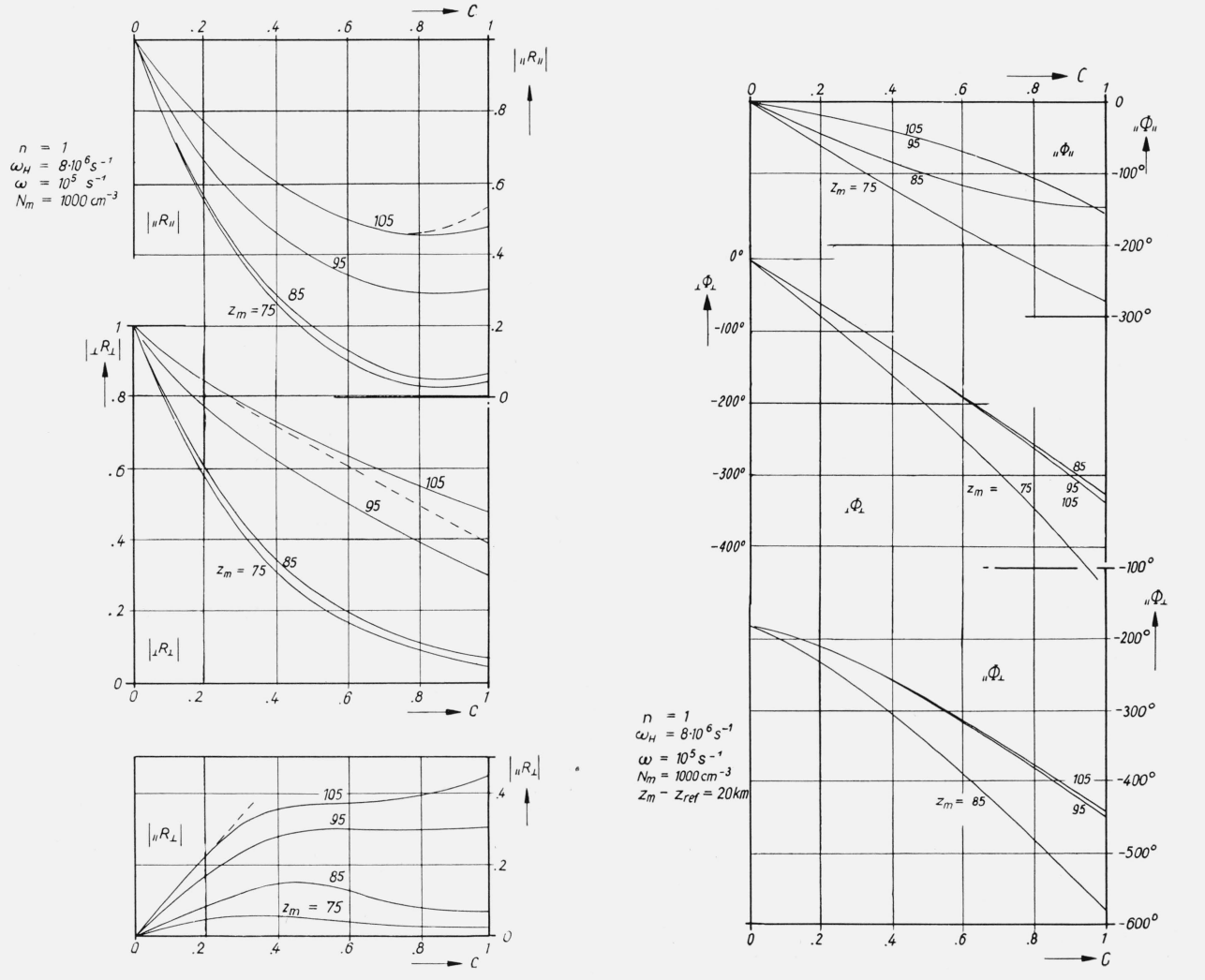

FIGURE 7. *Calculated amplitude (fig. 7a) and phase (fig. 7b) of the elements of the reflection matrix for different ionospheric models.*

are more uncertain than the values of the daytime ionosphere, especially the phase.

The results of calculation of the elements of **R** for the parameters $N_m=10^3$ cm^{-3} and $z_m=75$, 85, 95, and 105 km are shown in figure 7a (amplitude) and figure 7b (phase). Because of the special choice of the direction of the geomagnetic field, ${}_{\perp}R_{||}={}_{||}R_{\perp}$. The elements of **R** are represented as

$$R=|R|e^{j(\pi+\phi)}. \tag{19}$$

In figure 7b, ϕ is plotted versus $C=\cos\zeta$.

From the phase ϕ an equivalent reflection height h' can be defined [Budden, 1961a]:

$$h'=z_{\mathrm{ref}}-\frac{1}{2k}\left\{\frac{\partial\phi}{\partial\cos\zeta}\right\}_{\zeta=\zeta_0}. \tag{20}$$

z_{ref} is an arbitrary reference height of the calculated phase. In our example, it is

$$z_{\mathrm{ref}}=z_m-20\text{ km}. \tag{21}$$

Thus, it is inferred that spherical waves at angle of incidence ζ_0, are reflected at height h' with a reflection coefficient of amplitude $|R|$ and a phase jump of 180°. It is to be noted that h' depends on the angle of incidence ζ. In figure 8, h' calculated from the data in figure 7b in conjunction with (20) is plotted versus z_m for oblique incidence ($\cos\zeta<0{,}3$) and vertical incidence ($\cos\zeta=1$). The slope of h' is different at vertical and oblique incidence for the same ionospheric model. Qualitatively, the same phenomenon has been observed by Bracewell et al.

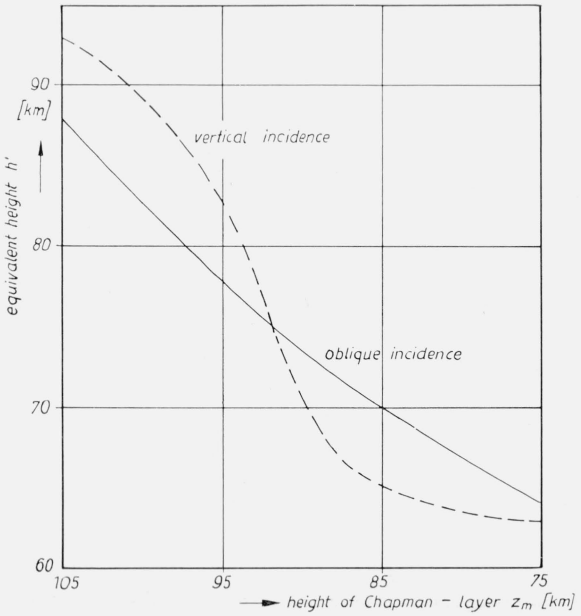

FIGURE 8. *Equivalent height* h′ *versus height of Chapman-layer* z_m *deduced from the ionospheric models in figure 7b for vertical incidence* (C=1) *and oblique incidence* (C<0.3).

[1951] for the transition from night to day. As can be seen from figure 8, Bracewell's interpretation of the phenomenon [Bracewell and Bain, 1952] assuming two different D layers seems to be unnecessary.

At the oblique incidence ($\cos\zeta<0{,}3$), it is seen that

$$\frac{\partial\phi}{\partial\cos\zeta}\approx\text{constant}. \tag{22}$$

This means that h' is constant for $\cos\zeta<0{,}3$. Now, $\cos\zeta=0{,}3$ is equivalent to a distance of $\rho=450$ km for $h'=70$ km. Therefore, it is possible to operate with a constant equivalent height in the whole region of medium and large distances. This fact facilitates the introduction of an isotropic and homogeneous equivalent of the ionosphere which behaves like the inhomogeneous and anisotropic ionosphere for plane waves at oblique incidence and a given frequency. This equivalent has an effective conductivity σ and an effective dielectric constant ϵ, so that $|{}_{||}R_{||}|$ and $|{}_{\perp}R_{\perp}|$ are the same for the inhomogeneous ionosphere and the surrogate at $\cos\zeta<0{,}3$. Since the phase of the reflection coefficient of a homogeneous ionosphere with sharp boundary at oblique incidence differs from 180°, the equivalent ionosphere must have the virtual height h which is slightly different from h' [Volland, 1964a]. For ${}_{||}R_{\perp}$, the statement

$${}_{||}R_{\perp}\approx\gamma Ce^{2jk(h-h')C}\qquad(C<0{,}3) \tag{23}$$

is appropriate. The phase term in (23) relates the phase of ${}_{||}R_{\perp}$ to the height h of ${}_{||}R_{||}$. In figure 7a, some calculated reflection coefficients of the equivalent are drawn as dashed lines which fit to the corresponding values of the models with the parameter $z_m=105$ km. All parameters of the equivalent of the models in figure 7 are put together in table 1. We see that ϵ can take negative values.

TABLE 1. *Parameters of equivalent ionospheres which at oblique incidence and 16 kc/s have the same reflection characteristics as the inhomogeneous and anisotropic ionospheric models* (h′,h, *and* z_m *in km*)

z_m	75	85	95	105
$\epsilon({}_{||}R_{||})$	1.0	0.9	0.4	−0.4
$\epsilon({}_{\perp}R_{\perp})$	3.5	3.0	0.9	0.2
$\frac{\sigma}{\epsilon_0\omega}({}_{||}R_{||})$	1.0	1.0	1.0	1.0
$\frac{\sigma}{\epsilon_0\omega}({}_{\perp}R_{\perp})$	1.0	1.0	1.0	1.0
γ	0.3	0.4	0.9	1.1
$h'({}_{||}R_{||})$	63	70	78	88
$h'({}_{||}R_{\perp})$	----------	69	82	92
$h'({}_{\perp}R_{\perp})$	65	73	83	93
$h({}_{||}R_{||})$	63	70	77	87
$h({}_{\perp}R_{\perp})$	68	76	85	95

In this manner each arbitrary ionospheric model can be substituted by a homogeneous ionosphere with a sharp boundary which has the same reflection characteristics as the model at oblique incidence and a given frequency.

The influence of the geomagnetic field increases with increasing height z_m and with increasing $\cos \zeta$. At $C=1$, even for low values of z_m (daytime conditions), it yields $|_{\|}R_{\|}|=|_{\perp}R_{\perp}|\approx|_{\|}R_{\perp}|$. The reflected waves, therefore, have nearly circular polarization. With decreasing C, the value

$$\frac{|_{\|}R_{\perp}|}{|_{\|}R_{\|}|}$$

decreases. This is the reason for the small influence of the geomagnetic field on VLF at oblique incidence.

Since h and h' are constants at oblique incidence, the equivalent ionosphere can be applied for the calculations at mode theory, too. The effective parameters of the equivalent ionosphere h', σ, and ϵ strongly depend on frequency [Volland, 1963]. Therefore, it is necessary to repeat the calculation of **R** for the same model at other frequencies.

3.2. Propagation Formula

The theory of propagation of VLF waves in plane or curved waveguides with sharp boundaries has been treated extensively. Detailed information may be found in the books of Budden [1961b] and Wait [1962]. In the VLF range, the transmitter antennas mostly behave like vertical electric dipoles. In what follows it is assumed that both transmitter and receiving antennas are situated on the ground.

The vertical component of the electric field strength of a vertical electric dipole according to a simplified form of mode theory is [Volland, 1964a]

$$E_z \cong 2E_0 \sqrt{\frac{\theta}{\sin\theta}} \frac{\sqrt{\rho\lambda}}{h} \sum_{n=1}^{\infty} S_n^{3/2} \cosh^2 A_{en} e^{jk\rho\left(1-S_n-\frac{h}{2a}S_n\right)-j\frac{\pi}{4}} \quad (24)$$

with

$$A_{en}=-\frac{1}{2}\ln R_e(C_n)\approx\frac{1}{n_e\overline{C}_n}$$

$$C_n=\overline{C}_n+\frac{j}{kh}\Delta_n \text{ (eigenvalue of the } n\text{th mode)}$$

$$\overline{C}_n=\frac{(n-1/2)\pi}{kh}$$

$$\Delta_n\cong\frac{n_i^2\overline{C}_n}{\sqrt{n_i^2-\overline{S}_n^2}}+\frac{1}{n_e\overline{C}_n}+\frac{\gamma^2\overline{C}_n^2}{4}e^{4n_i\overline{C}_n+\frac{2}{n_e\overline{C}_n}}$$

$$S_n=\sqrt{1-C_n^2}\approx 1-\frac{1}{2}\left(\overline{C}_n^2+2j\frac{\overline{C}_n\Delta_n}{kh}\right)$$

$n_i=\left(\epsilon-\frac{j\sigma}{\epsilon_0\omega}\right)^{1/2}$ (refraction index of the homogeneous equivalent ionosphere)

$n_e\cong\left(\frac{-j\sigma_e}{\epsilon_0\omega}\right)^{1/2}$ (refraction index of the homogeneous earth)

ϵ, σ, h = effective parameters of the ionosphere
σ_e = conductivity of the earth
ω = angular frequency
θ = angular distance between transmitter and receiver
a = earth radius
E_0 = undisturbed electric field strength of a vertical dipole in free space and distance ρ.

The mode factors

$$B_n=\sqrt{\frac{\theta}{\sin\theta}}\,e^{-\frac{jhk\rho}{2a}S_n} \quad (25)$$

take into consideration the curvature of the earth. Since $S_n\approx 1$, B_n can be drawn before the sum in (24) as a common factor:

$$B=\sqrt{\frac{\theta}{\sin\theta}}\,e^{-\frac{jhk}{2a}\rho}. \quad (26)$$

For a first approximation, it is sufficient to neglect the imaginary part of S_n in (24). The phase of the nth mode then becomes

$$\varphi_n=\left(\frac{\overline{C}_n^2}{2}-\frac{h}{2a}\right)k\rho-\frac{\pi}{4}. \quad (27)$$

In this formula, it is remarkable that the phase retardation of the nth mode relative to the undisturbed propagation is compensated by the influence of the curved earth on account of

$$\overline{C}_n^2\approx h/a$$

for low order modes. This means that the phase velocity of the first mode

$$v_1=\frac{c}{1-\frac{1}{k}\frac{\partial\varphi_1}{\partial\rho}}=\frac{c}{1-\frac{1}{2}\left(\overline{C}_1^2-\frac{h}{a}\right)} \quad (28)$$

which is greater than the velocity of light c at frequencies below 8 kc/s [Jean et al., 1960] can become smaller than c at greater frequencies [Wait and Spies, 1961]. A more exhaustive discussion of this phenomenon is given by Wait [1962] who employs higher order approximations. He indicates that the equation is qualitatively correct.

The difference between daytime and nighttime

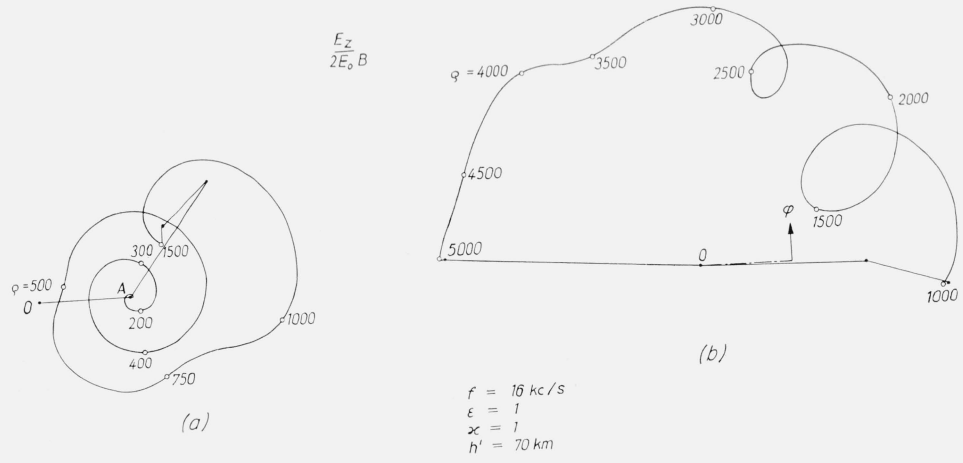

FIGURE 9. *Polar diagram of* $E_z/2E_0B$ *for the daytime model depending on distance.*

(a) The left hand diagram is calculated by ray theory. (b) The right hand diagram is calculated by mode theory.

phase of the first mode, according to the simplified theory, is

$$\varphi_{\text{night}}-\varphi_{\text{day}}\cong -k\rho\left\{\frac{\pi^2}{8k^2}\left(\frac{1}{h^2_{\text{day}}}-\frac{1}{h^2_{\text{night}}}\right)+\frac{h_{\text{night}}-h_{\text{day}}}{2a}\right\}. \tag{29}$$

The influence of the geomagnetic field is placed into the values ϵ, σ, and γ. Now the magnitude of the third term of Δ_n is very small compared with the other terms on account of $\overline{C}_n^2/4<<1$ and may be neglected. The consequence is that in the ray theory approximation the terms with ${}_{\shortparallel}R_{\perp}$ and ${}_{\perp}R_{\shortparallel}$ also may be neglected. The corresponding formula of ray theory, therefore, is

$$E_z\cong 2E_0B\left(W+2\sum_{n=1}^{\infty}\sin^3\zeta_n\left(\frac{1+R_e}{4}\right)^2 R_e^{n-1}|_{\shortparallel}R_{\shortparallel}|^n e^{jk(\rho-r_n)-jn\pi}\right) \tag{30}$$

where the Sommerfeld function W is replaced by unity, $\sin\zeta_n=\frac{\rho}{r_n}$, $r_n=\sqrt{\rho^2+(2nh')^2}$, h'=equivalent height, $|_{\shortparallel}R_{\shortparallel}|$=amplitude of the reflection coefficient of the inhomogeneous and anisotropic ionosphere, and, finally, R_e=reflection coefficient of the earth for vertically polarized waves.

The curvature of the earth has been taken approximately into consideration by the factor B (see (26)). If we assume the earth's surface to be ideally conductive ($A_{en}=0$; $R_e=1$), the resultant error primarily influences the amplitude of E_z. In the following calculations we shall make this assumption. The neglect of the finite conductivity of the earth, however, is allowed for only up to frequencies of about 20 kc/s.

3.3. Interpretation of the Diurnal Phase Measurements

With help of the propagation formulae (24) and (30) together with the ionospheric parameters given in table 1, the field strength E_z has been calculated depending on distance ρ. As the daytime model, the model with the parameters $N_m=1000$ cm^{-3} and $z_m=85$ km ($h'=70$ km) was selected. The reason for the choice of this model may be seen in section 3.5. For the nighttime, the model with the parameters $N_m=1000$ cm^{-3} and $z_m=105$ km has been used. For convenience, an equivalent height of $h'=90$ km instead of 88 km, according to table 1, has been introduced.

The calculations have been made by (30) up to $\rho=1500$ km and by (24) above $\rho=1000$ km. The agreement of the results in the range between 1000 and 1500 km served as control. The calculated difference $-\Delta\varphi_m$ is shown in figure 2 as a continuous full line. Comparing the calculated curve with the experimental data, we see that an agreement is possible only if we take two jumps of 360° at $\rho=600$ km and $\rho=2600$ km. This discrepancy can be explained, if we plot $E_z/2E_0B$ in a polar diagram. This is shown in figure 9 for daytime propagation and in figure 10 for nighttime propagation. Figure 9a originates from the ray theory (30). The straight line $0A$ corresponds to the groundwave (assuming $W=1$). The thin straight lines—drawn in figure 9a only for the case $\rho=1500$ km—correspond to the multihop skywaves. The portions of the skywaves increase with increasing distance. The vector drawn from the point 0 to an end point of the curve gives amplitude and phase of $E_z/2E_0B$. Figure 9b is originated by mode theory (24). Here the straight lines correspond to the mode terms. The modes of higher order decrease with increasing distance. Figure 10 must be read in the same manner.

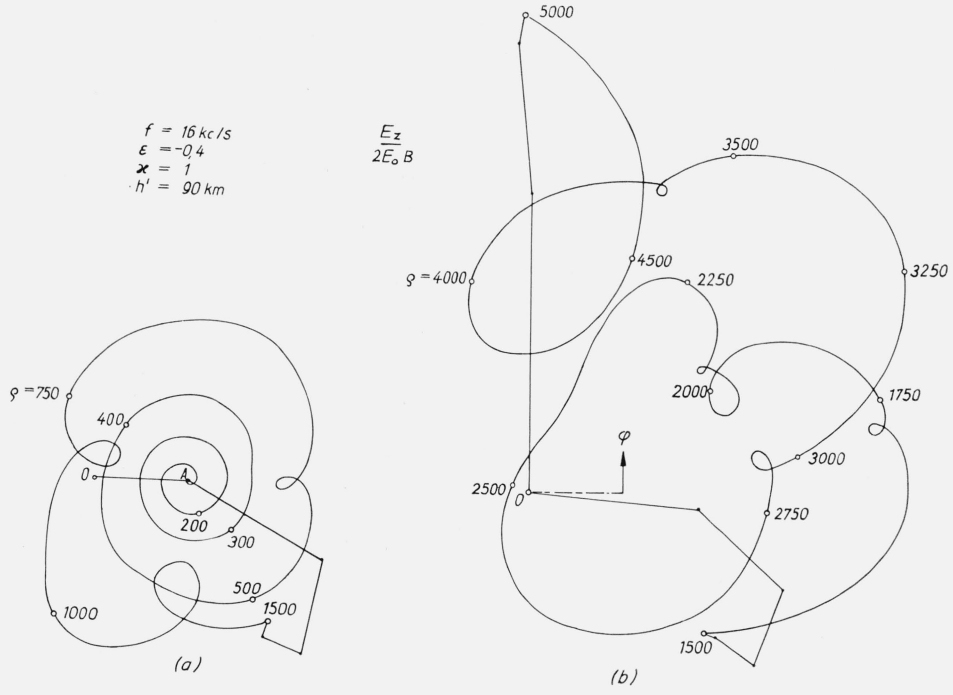

FIGURE 10. *Polar diagram of* $E_z/2E_0B$ *for the nighttime model depending on distance.*

(a) The left hand diagram is calculated by ray theory. (b) The right hand diagram is calculated by mode theory.

From figure 9a and 10a, we see that between 500 and 1000 km the origin 0 will be encircled by the endpoint of the vector in a clockwise sense at daytime and in a counterclockwise sense at nighttime. The nighttime phase, therefore, receives a gain of 360° or one wavelength in respect to the daytime phase. We would obtain such a result if the measurements were made by a synchronized oscillator in an aircraft flying off the transmitter at daytime and nighttime, respectively. Yet, there exist only few measurements of this kind [Reder et al., 1961]. All measurements plotted in figure 2 are made at one location. By this fact the phenomenon is hidden.

Figure 11 shows two polar diagrams for two constant distances, $\rho=600$ km and $\rho=650$ km. Here it was assumed that the equivalent height h' and the corresponding ionospheric parameters in table 1 changed continuously from the nighttime value to the daytime value. We would expect such picture if we would measure continuously, phase and amplitude at one location. As can be seen from figure 11, the origin is circulated in a left hand sense at the smaller distance and in a right hand manner at the larger distance. There must exist a distance between both these distances where the vector runs through the origin. The phase becomes indefinite. In this range, the measured diurnal phase lag jumps by 360° from negative to positive values. This is indicated in figure 2 by the vertical dashed line at 600 km. Receiver stations situated round this critical distance may fall from the positive into the negative phase lag region, or vice versa, if the reflection characteristics of the nighttime ionosphere changes from one night to the next. The phase difference must then differ rather exactly by 360°. This is the qualitative interpretation of the phase anomaly observed in Lindau (see fig. 3).

In our model, a second phase gain of 360° of the nighttime phase occurs at 2600 km. Here the sum of the second and higher order modes is larger than the first order mode and is phase shifted by 180°. The magnitude of the minimum of $-\Delta\varphi_m$ in this region depends very sensitively on the minimum difference vector of the modes at nighttime. Unfortunately, the measurements in these distances are insufficient to decide whether the second phase gain is real or not. In any case, phase measurements in

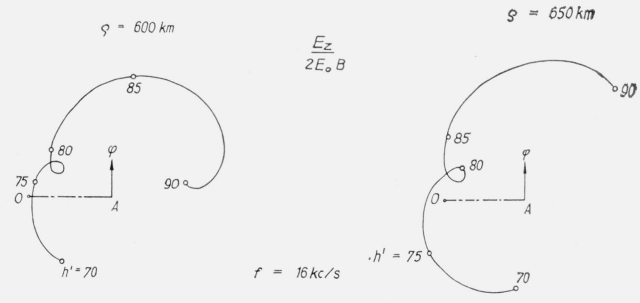

FIGURE 11. *Polar diagram of* $E_z/2E_0B$ *depending on equivalent height* h′ *for two different distances* $\rho=600$ *km and* $\rho=650$ *km.*

these two regions give very sensitive indications of the diurnal and interdiurnal change of the lower ionosphere.

The agreement between measurements and calculation in figure 2 can be only of qualitative kind because the measurements are made at different times, different regions and different frequencies. The dash-dotted line in figure 2 is the calculated phase lag of the first mode, according to (29). We see that up to 5000 km the second mode may not be neglected for the nighttime propagation.

The value $-\Delta\tau_m/\rho$ calculated from (29) for the first mode is shown in figure 3 as a dashed line. Here a nighttime height, $h'_{night}=88$ km, has been chosen. The theoretical curve fits well with the measured values. No attempt has been made to explain the minimum at 16 kc/s, since the number of measured frequencies in the region is very small.

3.4. Interpretation of the Sunrise Effects

The model previously used is valid only if it is able, also, to explain the transition from night to daytime conditions. At shorter distances, when the one hop skywave exists primarily besides the groundwave, it seems to be appropriate to approximate the transition by lowering the whole ionosphere continuously. In figure 12a, calculated values of $E_z/2E_0B$, according to ray theory, are plotted in the usual manner for the distance $\rho=980$ km and different heights h'. Amplitude and phase from figure 12a are drawn separately in figure 12b as full lines versus h'. Here the phase term of B has been added to the phase. The dashed lines in figure 12b are amplitude and phase of GBR measured in Berlin on December 12, 1962. This sunrise effect represents well the monthly means in figure 5. The scale of h' of the theoretical curve and the time scale of the measured values are related in such a manner that the two curves fit best. The sunrise effect begins at a zenith distance of $\chi=99°$ at the middle of the propagation path and ends at $\chi=93.5°$. The agreement between calculation and measurements is very good. It is worth mentioning that the scaled h' must not be proportional to the registration time.

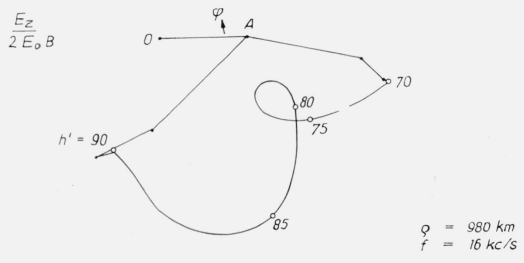

FIGURE 12a. *Polar diagram of* $E_z/2E_0B$ *depending on equivalent height* h' *for* $\rho=980$ *km.*

The sunrise effect in summer (see fig. 5) cannot be explained as well as the winter effect. But we get a qualitative agreement between calculation and measurement, when we assume that in summer the nighttime ionosphere ends at $h'=85$ km. Then the deep minimum of amplitude and the turning point of phase caused by the interference between one hop and two hop wave remain, but the amount of amplitude is too small in respect to the measured values. If we suppose a larger amplitude of skywaves in summer, we even get quantitative agreement.

A likewise qualitative agreement exists between measured and calculated sunrise effect at distances of 2150 km. In figure 13, a diurnal phase change of GBR measured in Malta ($\rho=2150$ km) by Blackband [1961] has been plotted together with calculated data according to our model for the transition from night to day. The course of phase is the result of interference between first and second mode. We cannot expect better agreement, since the validity of our transition model begins to cease at these distances.

3.5. Interpretation of Daytime Phase variations and Solar Flare Effects

The normal variation of equivalent height at daytime is caused by the variation of the electron density profile of the lower ionosphere. During a solar flare, the illuminated part of the lower ionosphere becomes additionally ionized, and therefore the equivalent height is lowered for a short time. If one assumes that the region of the lower ionosphere where the reflection of the VLF waves takes place behaves approximately like a monochromatic Chap-

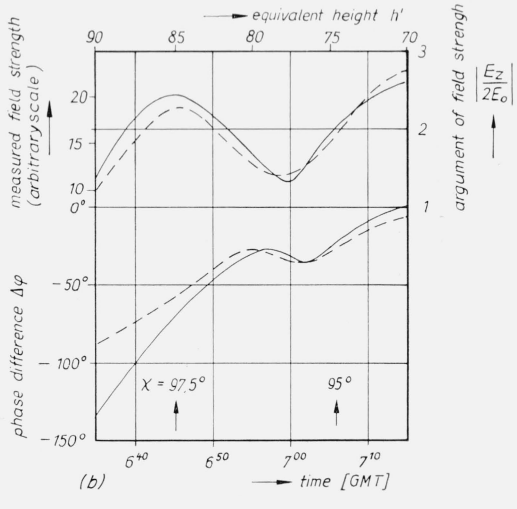

FIGURE 12b. $E_z/2_0E$ *from figure 12a, amplitude and phase separated, versus equivalent height* h' *(full line).*

The dashed lines are amplitude and phase of GBR field strength during sunrise versus time observed in Berlin on December 12, 1962. The arrows indicate time of zenith distance χ at the middle of the propagation path.

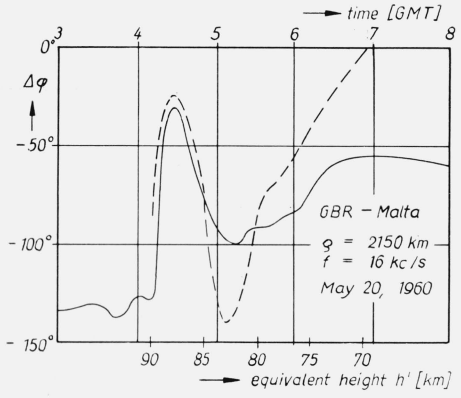

FIGURE 13. *GBR phase during sunrise versus time observed in Malta on May 20, 1960, according to Blackband [1961] (full line).*

The dashed line is the calculated phase versus equivalent height h'.

man layer, then the daytime variation of the electron profile is caused by the variation of zenith distance χ of the sun. On the other hand, during a solar flare, the additional solar emission at nearly constant zenith distance can be expected to increase the strength of the layer without changing its shape.

Recently, however, this conception has been questioned by Friedman [1960], who indicated that a new layer caused by X-rays is built up during a solar flare. In the following, only the first conception of one layer will be used. For the second conception of two layers [see Volland, 1964b].

Ionospheric reflection coefficients ${}_{||}R_{||}$ have been calculated for 16 kc/s and a number of ionospheric models with electron profiles like (16) and collision number profiles like (17) [Volland, 1963]. The chosen parameters were $z_m=75$ and 85 km and N_m between 100 and 10^5 cm^{-3}. From this calculation it follows that the amplitude $|{}_{||}R_{||}|$ does not change very markedly (see the values of $|{}_{||}R_{||}|$ in fig. 7a for $z_m=75$ and 85 km). On the other hand, the phase and therefore h' show essential variations.

A sharply bounded homogeneous surrogate ionosphere with parameter $n_i^2=1-j$ has nearly the same value $|{}_{||}R_{||}|$ as the inhomogeneous models at oblique incidence. The imaginary part of n_i^2 is

$$\frac{\sigma}{\epsilon_0\omega}=1. \tag{31}$$

Moreover, we state the well-known relation for very low frequencies

$$\sigma=\frac{e^2N}{m\nu}=2.81\cdot10^{-8}\,\frac{N}{\nu}\ \text{mho/m} \tag{32}$$

(e and m are charge and mass of electron).

We now fix that height z_a within the inhomogeneous ionosphere where (31) and (32) yield:

$$\frac{N(z_a)}{\nu(z_a)}=\frac{\epsilon_0\omega}{2.81}\cdot10^8=31.5m^{-3}s \tag{33}$$

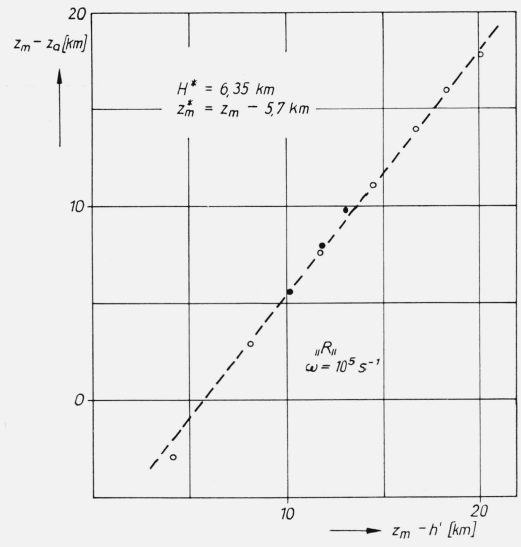

FIGURE 14. *Relation between equivalent height* h′ *and the height* z_a *of the point* $N=31.5\nu$ *of a Chapman-layer in the height* z_m *at frequency* $f=16$ *kc/s.*

Points and circles are calculated from the reflection coefficients ${}_{||}R_{||}$ of different models. The dashed straight line is

$$\frac{z_m-z_a}{H}=\frac{z_m-h'}{H^*}$$

and calculate the difference z_m-z_a. If we plot this value versus the difference z_m-h' of the same model, we get figure 14. The points gained from the different models nearly lie on the straight line

$$\frac{z_m-z_a}{H}=\frac{z_m^*-h'}{H^*} \tag{34}$$

with $H=8$ km (scale height), $H^*=6.35$ km (equivalent scale height), and $z_m^*=z_m-5.7$ km (equivalent characteristic height). If $(z_m-z_a)/H$ is replaced by $(z_m^*-h')/H^*$ in

$$\frac{N(z_a)}{\nu(z_a)}=\frac{N_m}{\nu_m}\exp\left\{\frac{1}{2}\left[1-\frac{2(z_m-z_a)}{H}-\exp\frac{(z_m-z_a)}{H}\right]\right\}=31.5 \tag{35}$$

it is seen that each measured value of h' corresponds to a height z_a where $N=31.5\nu$. Since ν is supposed to be known, we are able to determine N in the height z_a from the measured value of h'. For 16 kc/s and oblique incidence, the lower ionosphere in daytime, therefore, behaves like a sharply bounded homogeneous ionosphere with refractive index $n^2=1-j$. Its height h' is in the point $N=31.5\nu$ of a transformed Chapman layer with the parameters N_m, z_m^*, and H^*.

In view of the relation

$$z_m = z_{m_0} - H \ln \cos \chi \tag{36}$$

where z_{m0} is the characteristic height of the Chapman layer at zero zenith distance, it follows from (35) that

$$\ln \frac{1}{\cos \chi} = \frac{h' - z^*_{m0}}{H^*} + \ln \left\{ 1 - 2 \ln 31.5 \frac{\nu_{m0}}{N_{m0}} + 2 \left(\frac{h' - z^*_{m0}}{H^*} \right) \right\}. \tag{37}$$

This equation makes possible the determination of z_{m0} and $\frac{\nu_{m0}}{N_{m0}}$, if the daytime variation of h' is known. Figure 15 shows values of h' determined from the field strength of GBR measured in Berlin between April and June 1959 [Volland, 1959]. The dashed line is calculated from (37) with help of the parameters: $z_{m0}=85$ km, $N_{m0}=10^9$ m$^{-3}=1000$ cm^{-3}, $\nu_{m0}=1.5 \cdot 10^6$ s^{-1} in 85 km height (see (17)). At the reflection point of the one hop wave at local noon in May, it is $\cos \chi = 0.82$. From this it follows that $z_m = 86.5$ km and $N_m = N_{m0} = 1000$ cm^{-3} which is in good agreement with the daytime model hitherto used.

During a solar flare, the parameter N_m is changing at constant z_m. The retardation of N in respect to the solar emission is governed by the equation

$$\frac{dN}{dt} = q_0 (1 + \delta e^{-\gamma t}) - \alpha N^m \qquad (t \geqq 0) \tag{38}$$

for $m=1$ or 2. Here q_0 is the normal ion production rate prior to the onset which is considered to remain constant during the flare; δ is the maximum relative increase of ion production rate; $e^{-\gamma t}$ is the ideal time course of a typical solar flare; and γ is the decay constant. In (38), $m=2$ corresponds to the effective recombination in which case α is a recombination coefficient. On the other hand, $m=1$ corresponds to effective attachment. In which case, α is an effective attachment coefficient.

Neglecting vertical motion of electrons and presuming values of γ, δ, α, and m, the momentary relative increase of electron density

$$x = \frac{\Delta N(z, t)}{N_0(z)} \tag{39}$$

can be calculated from (38) for each height z, depending on time Δt from the beginning of the effect. The height z_a can be determined from these electron profiles and from (33). Likewise the difference $\Delta h' = h'(t) - h'_0$ can be calculated from (34). Otherwise $\Delta h'(t)$ can be determined from measurements during a solar flare. Figure 16 shows as an example $\Delta h'$ versus Δt. The points are measured values of a solar flare effect. The full line is evaluated with help of the parameters:

$$\begin{aligned} &\delta = 85 \\ &\gamma = 7.2 \cdot 10^{-3} s^{-1} \\ &\alpha = 2.2 \cdot 10^{-3} s^{-1} \text{ in 70 km height} \\ &m = 1. \end{aligned} \tag{40}$$

Here it was presumed

$$\alpha \propto e^{-z/H}. \tag{41}$$

The combination of parameters (40) is unique, since the curve must fit both height and time of maximum and the decay of the measured values with time.

Similar calculations have been done for 15 additional selected solar flare effects [Volland, 1964b]. The selection was taken in such a way that only solar

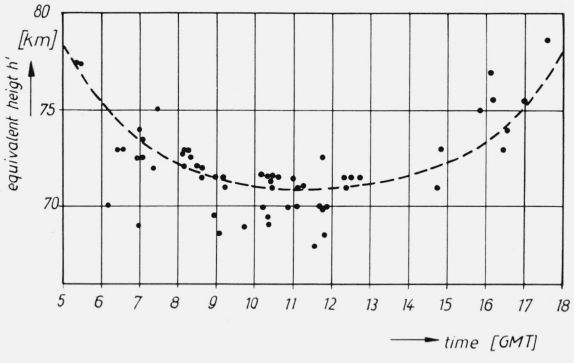

FIGURE 15. *Equivalent height* h' *determined from field strength measurements of GBR in Berlin between April and June, 1959, versus time (points) and theoretical curve (dashed line).*

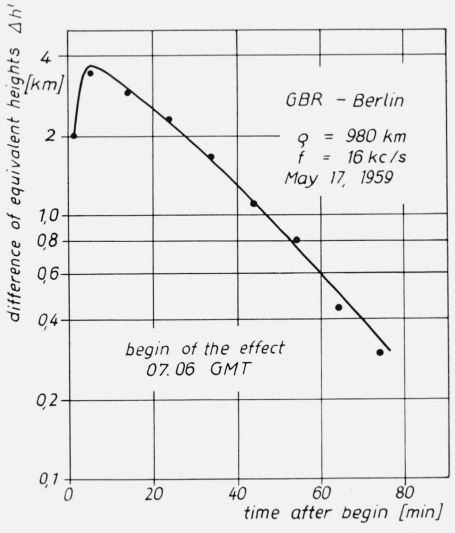

FIGURE 16. *Course of departure of equivalent height from the normal value* Δh' *during a solar flare determined from field strength measurements of GBR in Berlin (points) and theoretical curve (full line) versus time after beginning of the solar flare.*

flares were used which had the proposed course of emission according to (38). To decide this question, the 3.2 cm solar radio emission which is supposed to behave very similarly, has been used. Twelve of the fifteen effects could be interpreted quantitatively by (38) only with the parameter $m=1$. The medium value of the attachment coefficient is

$$\alpha=3.4\cdot10^{-3}s^{-1} \qquad \text{in 70 km height}$$

in agreement with results of HF-absorption measurements during SID's [Taubenheim, 1962]. The rest were very strong effects with maximum height differences $\Delta h'$ of more than 9 km. The effective attachment law therefore seems to be valid in this height.

4. References

Blackband, W. T. (Nov.–Dec. 1961), Effects of the ionosphere on VLF navigation aids, J. Res. NBS 65D (Radio Prop.), No. 6, 575–580.

Blackband, W. T. (1962a), Diurnal phase changes in the arctic propagation of VLF-waves, Tech. Note No. RAD 814, Royal Aircraft Establishment, Farnborough.

Blackband, W. T. (1962b), Diurnal changes in the transmission time for VLF sky wave signals, Tech. Note No. RAD 816, Royal Aircraft Establishment, Farnborough.

Bracewell, R. N. (1952), The ionospheric propagation of radio waves of frequency 16 kc/s over distances of about 200 km, Proc. IEE **99,** 217.

Bracewell, R. N., and W. G. Bain (1952), An explanation of radio propagation at 16 kc/s in term of two layers below the *E*-layer, J. Atmospheric Terrest. Phys. **2,** 216–225.

Bracewell, R. N., K. G. Budden, J. A. Ratcliffe, T. W. Straker, and K. Weekes (1951), The ionospheric propagation of low and very low frequency radio waves over distances less than 1000 km, Proc. IEE **98,** 221.

Budden, K. G. (1961a), Radio waves in the ionosphere (Cambridge Univ. Press, Cambridge).

Budden, K. G. (1961b), The wave guide mode theory of wave propagation (Logos Press, London).

Casselmann, C. J., D. P. Heritage, and M. L. Tibbals (1959), VLF propagation measurements for the Radux-Omega navigation system, Proc. IRE **47,** 829–859.

Chilton, C. J., D. D. Crombie, and A. J. Jean (1962), Phase variations in VLF propagation, AGARD Meeting, Munich.

Crombie, D. D. (May–June 1960), On the mode theory of very-low-frequency propagation in the presence of a transverse magnetic field, J. Res. NBS **64D** (Radio Prop.), No. 3, 265–267.

Crombie, D. D. (Sept.–Oct. 1961), Reflection from a sharply bounded ionosphere for VLF propagation perpendicular to the magnetic meridian, J. Res. NBS **65D** (Radio Prop.), No. 5, 455–463.

Crombie, D. D., A. H. Allan, and M. Newman (1958), Phase variations of 16 kc/s transmissions from Rugby as received in New Zealand, Proc. IEE **105**, 301–304.

Eppen, F., and G. Heydt (1959), Eine Registrieranlage für Längstwellen, Techn. Bericht des Heinrich-Hertz-Instituts, Nr. 35, Berlin-Charlottenburg.

Friedman, H. (1960), The sun's ionizing radiation from Physics of the Upper Atmosphere, ed. by J. A. Ratcliffe (Academic Press, London).

Ginzburg, V. L. (1961), Propagation of electromagnetic waves in plasma, 89 ff. (North Holland Publishing Co., Amsterdam).

Hampton, D. E., and A. S. Hill (1962), The statistical prediction of diurnal phase changes, AGARD Meeting, Munich.

Jean, A. G., W. L. Taylor, and J. R. Wait (1960), VLF phase characteristics deduced from atmospheric waveforms, J. Geophys, Res. **65,** 907–912.

Nicolet, M. (1959), The constitution and composition of the upper atmosphere, Proc, IRE **47,** 142–147.

Pierce, J. A. (1955), The diurnal carrier phase variations of 16 kc/s transatlantic signal, Proc. IRE **43,** 584–588.

Pierce, J. A. (1957), Intercontinental frequency comparison by very low frequency radio transmission, Proc. IRE **45,** 794–803.

Pierce, J. A., G. M. R. Winkler, and R. L. Corke (1960), The GBR experiment: a transatlantic frequency comparison between caesium-controlled oscillators, Nature **187,** 914–916.

Reder, F. H., M. R. Winkler, and C. Bickart (1961), Results of long range clock synchronization experiments, Proc. IRE **49,** 1028–1032.

Taubenheim, J. (1962), Information of the ionizing radiation of solar flares from the ionospheric absorption effect, J. Atmospheric Terrest. Phys. **24,** 191–201.

Utech, H., and J. Zahn (1961), Kontinuierlicher Phasenschieber zur Kompensation der Frequenzabweichung und Alterung der Normalfrequenzanlage des HHI, Tech. Bericht des Heinrich-Hertz-Instituts Nr 57, Berlin-Charlottenburg.

Volland, H. (1959), Die Frequenzabhängigkeit der Sonneneruptionseffekte im Längstwellengebiet, Arch. Elektr. Übertr. **13,** 443–448.

Volland, H. (July-Aug. 1961), Comparison between mode theory and ray theory of VLF, J. Res. NBS **65D,** (Radio Prop.), No. 4, 357–361.

Volland, H. (1963), Die Reflexion sehr langer elektromagnetischer Wellen am anisotropen und inhomogenen Ionosphärenplasma, Tech. Bericht des Heinrich-Hertz-Instituts Nr. 67, Berlin-Charlottenburg.

Volland, H. (1964a), Zur Theorie der Ausbreitung langer elektromagnetischer Wellen, Teil I und II, Arch. Elektr. Übertr. (in print).

Volland, H. (1964b), On the solar flare effect of VLF waves in the lower ionosphere, J. Atmospheric Terrest. Phys. (to be published).

Wait, J. R. (1961), A comparison between theoretical and experimental data on phase velocity of VLF waves, Proc. IRE **49,** 1089–1090.

Wait, J. R. (1962), Electromagnetic Waves in Stratified Media (Pergamon Press, London, and Macmillan, New York).

Wait, J. R. (1963), A note on diurnal phase changes of very low frequency waves for long paths, J. Geophys. Res. **68,** 338–340.

Wait, J. R., and K. R. Spies (1961), A note on phase velocity of VLF radio waves, J. Geophys. Res. **66,** 992–993.

Westfall, W. D. (1961), Prediction of VLF phase change and solar flare effects, J. Geophys. Res. **66,** 2733–2736.

(Paper 68D2–337)